Available online at www.sciencedirect.com
ScienceDirect
Global and Planetary Change 59 (2007) 126–137
GLOBAL AND PLANETARY CHANGE
www.elsevier.com/locate/gloplacha

Ice elevation and areal changes of glaciers from the Northern Patagonia Icefield, Chile

Andrés Rivera [a,b,*], Toby Benham [c,d], Gino Casassa [a], Jonathan Bamber [d,e], Julian A. Dowdeswell [c,d]

[a] *Centro de Estudios Científicos (CECS), Arturo Prat 514, Valdivia, Chile*
[b] *Departamento de Geografía Universidad de Chile, Santiago, Chile*
[c] *Scott Polar Research Institute, University of Cambridge, Cambridge, UK*
[d] *NERC Centre for Polar Observation and Modelling, UK*
[e] *Bristol Glaciology Centre, University of Bristol, Bristol, UK*

Available online 16 January 2007

Abstract

High thinning rates (up to -4.0 ± 0.97 m a^{-1}) have been measured at Campo de Hielo Patagónico Norte (CHN) or Northern Patagonia Icefield, Chile between 1975 and 2001. Results have been obtained by comparing a Digital Elevation Model (DEM) derived from regular cartography compiled by Instituto Geográfico Militar of Chile (IGM) based upon 1974/1975 aerial photographs and a DEM generated from Advanced Space-borne Thermal Emission and Reflection Radiometer (ASTER) satellite images acquired in September 2001. A complete cloud-free Landsat ETM+ satellite image mosaic acquired in March 2001 was used to update the available glacier inventory of the CHN, including all glaciers larger than 0.5 km^2 (48 new glaciers). A new delineation of ice divides was also performed over the accumulation areas of glaciers sharing the high plateau where the existing regular cartography exhibits poor coverage of topographic information. This updated glacier inventory produced a total ice area for 2001 of 3953 km^2, which represents a decrease of $3.4\pm1.5\%$ (140 ± 61 km^2 of ice) with respect to the total ice area of the CHN in 1979 calculated from a Landsat MSS satellite image. Almost 62% of the total area change between 1979 and 2001 took place in glaciers located at the western margin of the CHN, where the maximum area loss was experienced by Glaciar San Quintín with 33 km^2. At the southern margin, Glaciar Steffen underwent the largest ice-area loss (12 km^2 or 2.6% of the 1979 area), whilst at the eastern margin the greatest area loss took place in Glaciares Nef (7.9 km^2, 5.7% of the 1979 area) and Colonia (9.1 km^2, 2.7% of the 1979 area). At the northern margin of the CHN the lower debris-covered ablation area of Glaciar Grosse collapsed into a new freshwater lake formed during the late 1990s. The areal changes measured at the CHN are much larger than previously estimated due to the inclusion of changes experienced in the accumulation areas. The CHN as a whole is contributing melt water to global sea level rise at rates ~25% higher than previous estimates.

Keywords: Patagonia; glacier mapping; ASTER; DEM generation; remote sensing

1. Introduction

The Chilean Campo de Hielo Patagónico Norte (CHN), together with nearby Campo de Hielo Patagónico Sur (CHS), also known as the Northern and

* Corresponding author. Centro de Estudios Científicos (CECS), Arturo Prat 514, Valdivia, Chile. Tel.: +56 63 234543; fax: +56 63 234517.
E-mail address: arivera@cecs.cl (A. Rivera).

0921-8181/$ - see front matter © 2006 Elsevier B.V. All rights reserved.
doi:10.1016/j.gloplacha.2006.11.037

Southern Patagonian Icefields respectively, are the largest temperate icefields in the Southern Hemisphere (Warren and Sugden, 1993). They are considered to be amongst those glaciated areas which have contributed the largest proportion of melt water to sea level rise in the second part of the 20th century, due to thinning, frontal and areal changes experienced by their glaciers (Rignot et al., 2003). However, the contribution to sea level rise has been estimated based upon direct measurements of ice elevation and areal changes experienced mainly by the ablation areas of the CHN (Aniya, 1999). Unfortunately, data from the accumulation areas have been very sparse and, therefore, most previous studies have determined elevation changes by extrapolation from values measured in the ablation areas.

In this paper, we use ASTER images for DEM generation purposes, as well as Landsat imagery, in order to: (1) calculate the surface topography in the ablation and accumulation areas of the CHN; (2) compare ice elevation changes taking place in recent decades; (3) determine ice areal changes; (4) update and extend the existing glacier inventory; and (5) redefine the ice divides between the main glaciers of the CHN.

Among the glaciers of the CHN (latitudes 46.5°S and 47.5°S), San Rafael (Fig. 1A and B) is the only tidewater calving glacier (18% of the total CHN ice area), whilst the great majority (66% total area) have freshwater calving fronts. Both types of calving glaciers have been recognised as responding non-linearly to climate changes (Warren and Aniya, 1999). This anomalous behaviour is especially important when ice fronts are located in deep fjords or lakes, where ice tongues could reach a buoyancy point (for example due to thinning or longitudinal stretching) and subsequently generating massive calving events (Warren et al., 2001; Skvarca et al., 2002).

Most of the glaciers of the CHN have been retreating since the so-called Little Ice Age (LIA), which has been described as a sequence of advances experienced by Patagonian glaciers between AD 1600 and 1900 (Heusser, 1960; Winchester and Harrison, 1996). The position of many Patagonian glaciers in 1945 (when the first aerial photography was obtained) was similar to the moraines left during the last advances of the LIA, namely AD 1850–1900 (Harrison and Winchester, 1998). Since 1945, most of the glaciers were retreating (with exception of some advances in the 1990s), and most of the lower ends were thinning at high rates between 1945 and 1975 with an average rate between −1 and −2 m a^{-1} (Aniya, 1999). Unfortunately, most of these observations lack precise quantification and error budgets. Some other glaciers, including Glaciar Soler, have been measured more precisely, showing thinning rates between −0.7 and −2 m a^{-1} between 1983 and 1985 (Naruse, 1987) and a thinning of −3 m a^{-1} between 1985 and 1998 (Yamaguchi et al., 2003), in a trend that suggests acceleration of thinning in recent years.

The only previous quantification of ice elevation changes in the accumulation areas has been derived from estimates made by Rignot et al. (2003). These estimates were concentrated at low altitude, close to the ELA. The upper areas have only occasionally been visited due to logistic and weather difficulties (Matsuoka and Naruse, 1999). Aniya (1999) estimated a thinning between −0.5 and −1 m a^{-1} for the whole accumulation area of the CHN, based upon observation of thinning at the icefalls in the area of Glaciar Soler.

Due to the frequent bad weather conditions prevailing in the region of the CHN, only a few cloud-free vertical and hand-held oblique aerial photographs exist for the area. Recent cloud-free remotely-sensed imagery acquired from satellites is used here to account for the glacier area and elevation changes.

2. Data sets

2.1. Maps

Most ablation areas of the CHN are covered by the regular 1:50,000 scale maps published by the Instituto Geográfico Militar of Chile (IGM), which is based upon Mc Hurd aerial photography of 1975. Several point measurements carried out beyond the margin of the CHN were used as ground control by the IGM for the cartography. The lack of stereoscopic vision over flat snow-covered areas prevented contour line generation for most of the accumulation zones of the glaciers. The contour line interval on the maps is 50 m and many summits and spot heights are included. The original coordinate system of the cartography was UTM-18S South American 1969 (SAD-1969) datum. The vertical random error of this map was estimated as 17 m, by reference to the contour interval (Falkner, 1995). The horizontal random error was estimated as 15 m, based upon the National Imagery and Mapping Agency (NIMA, 1997) parameters for SAD-1969 regular cartography. The regular cartographic datum was converted to WGS-1984 using transformation parameters provided by IGM.

2.2. Satellite images

The earliest available cloud-free Landsat MSS image of CHN was acquired in January 22, 1979 (Table 1). Most satellite images covering the CHN over the

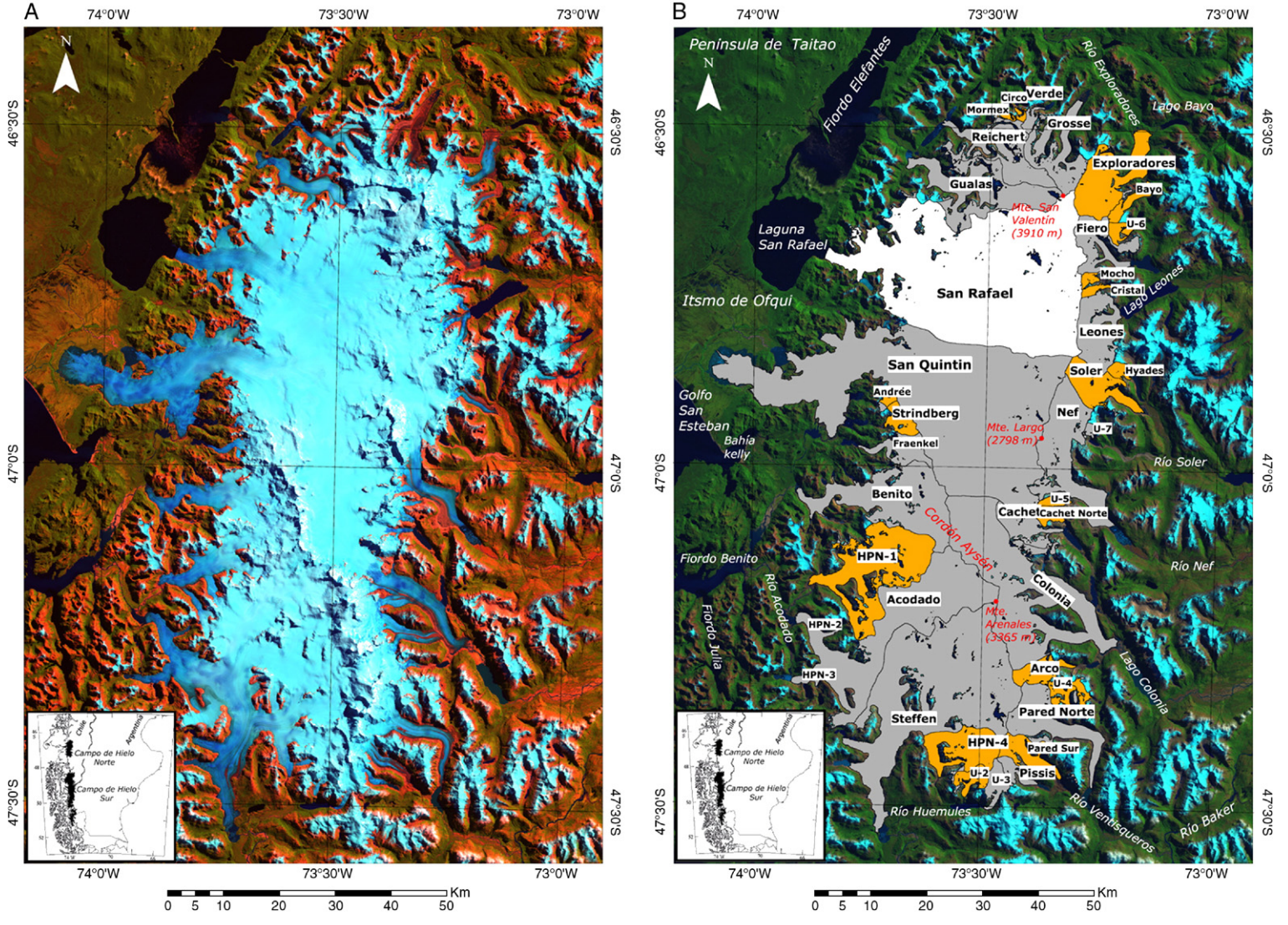

Fig. 1. A. The Campo de Hielo Patagónico Norte (CHN) or Northern Patagonia Icefield, Chile. False-colour composite of Landsat ETM+ satellite images mosaic, bands 1 (red), 4 (green) and 5 (blue), acquired on March 11, 2001. B. Main glacier basins of the CHN superimposed on the Landsat ETM+ mosaic of March 11, 2001 (in true colour). Tidewater glacier basin is shown in white, freshwater basins in grey and non-calving (or calving locally into small lagoons) in orange. Inset shows the location of the CHN and CHS in southern South America.

Table 1
Satellite images

Sensor	Acquisition date	Bands used in the analysis	Spatial resolution (m)	Source
Landsat MSS	1979, January 22	1, 2, 3 and 4	57 × 79	GLCF [b]
Landsat ETM+	2001, March 11	1, 4 and 5	28.5	USGS [c]
Terra ASTER	2001, September 3	1, 2, 3-Nadir (3N) and 3-Backward (3B) [a]	15	USGS [c]
Terra ASTER	2002, February 10	1, 2, 3-Nadir (3N) and 3-Backward (3B) [a]	15	USGS [c]

[a] Band 3-Backward (3B), is a near-infrared band obtained with a backward-looking angle of 27.6°.
[b] GLFC, Global Land Cover Facility, University of Maryland.
[c] USGS, United States Geological Survey.

intervening years are substantially cloud-covered. However, more recent scenes which displayed a minimum of cloud contamination include: (1) two Landsat ETM+ scenes (Fig. 1A and B) acquired on March 11th, 2001, path/rows (232/92 and 93); (2) three ASTER images acquired on September 3rd, 2001, (232/255, 256 and 257); and (3) two ASTER images acquired on February 10th, 2002, path/rows (232/256 and 257).

The Landsat MSS and ETM+ images were orthorectified by the Global Land Cover Facility of University of Maryland (GLCF) and the United States Geological Survey (USGS), respectively. The estimated absolute errors for these images are smaller than 50 m (Tucker et al., 2004).

The ASTER images were obtained as level L1A data from the USGS (Tables 1 and 2). For general assessment and use of the ASTER images, we applied the supplied radiometric and geometric parameters, yielding a georectification accuracy of <15 and <50 m as relative and absolute, respectively (Abrams et al., 2002). For use of the ASTER imagery in DEM production, the images were mosaiced within PCI Geomatica commercial software, and more accurate geolocation was performed as described later in this paper.

3. Methods

3.1. DEM generation from regular cartography

A reference DEM is required, based on the IGM cartography described in Section 2.1, in order to identify control point elevations for ASTER-DEM production and for the purpose of comparison with ASTER-derived DEM to establish rates of thinning.

The contour lines of the 50,000 scale regular cartography of 1975 were obtained directly from IGM in Arc View commercial software 8.2 digital format. Using "Topogrid" (Hutchinson, 1993), a bi-cubic spline interpolation procedure available from ARC INFO commercial software 8.2, a 50 m pixel size DEM was generated based upon these contour lines of the IGM. A jacknifing procedure (Lythe et al., 2001) was applied in order to determine the error induced by the interpolation process. The total vertical random error of the DEM was estimated to be 19 m by taking the square root of the sum of squared individual Root-Mean Square (RMS) error sources: 9 m due to the interpolation procedure (calculated using jacknifing) and 17 m due to inaccuracies of the contour lines.

3.2. DEM generation from ASTER images

Using PCI Geomatica commercial software, a DEM was generated using a mosaic of the three ASTER images acquired on September 3rd, 2001 (Table 2). More than 35 control points (CPs) were extracted from the IGM regular cartography for the DEM generation process. Approximately 80 tie points (TPs) were selected on the screen from all around the image mosaic, in order to constrain the orbit modelling. These points were selected from features observed in ASTER bands 3N (nadir-looking) and 3B (backward-looking), namely: moraines;

Table 2
ASTER image parameters

Acquisition date (Y/D/M)	Acquisition time (UTC)	Scene orientation angle in degrees	Satellite path	Solar elevation angle in degrees	Solar azimuth angle in degrees	Gain settings bands 3N and 3B	Data level type
2001/03/09	14:55:28.440	11.876	Descending	30.349	34.105	Normal	L1A
	14:55:37.309	11.993		29.754	34.026		
	14:55:46.179	12.113		29.366	34.148		
2002/10/02	14:50:23.954	11.993	Descending	46.514	53.077	Low	L1A
	14:50:32.825	12.113		46.269	52.773		

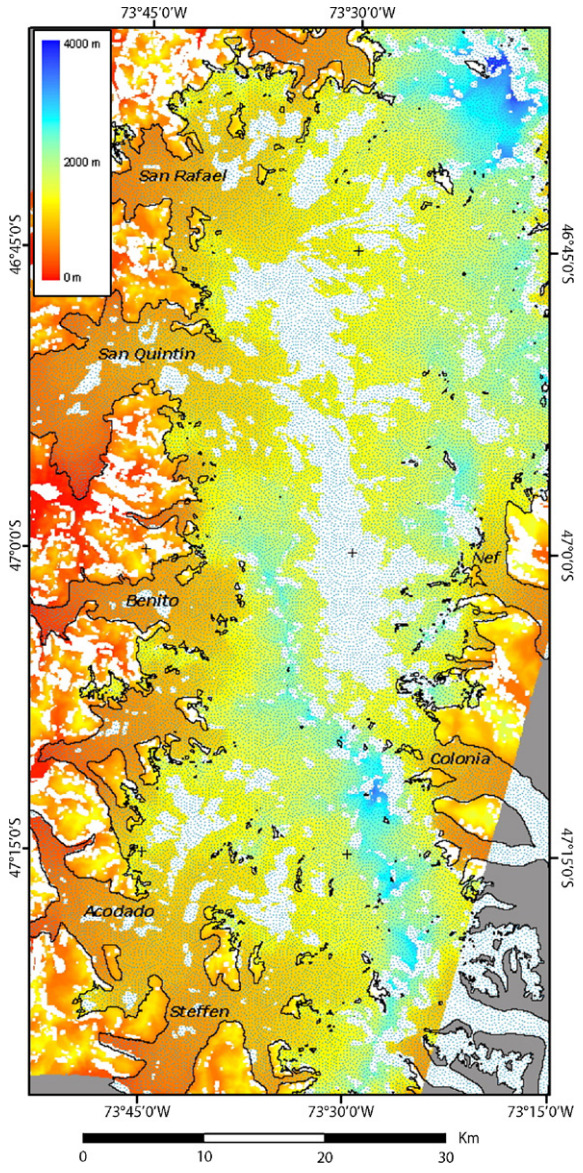

Fig. 2. ASTER-derived DEM of the central part of the CHN. Areas where inter-band stereo matching was not successful are in white. The small blue dots represent the ice area of the CHN. At the margins of the image, areas without ASTER-DEM coverage are in grey.

rock outcrops; ice crevasses; vegetation; rivers. By following the standard processes of epi-polar image pair production, DEM production, and geocoding, an absolute DEM (i.e. accurate in *XY* and *Z* co-ordinate values) was produced. The resulting DEM was edited manually in order to eliminate artefacts (speckle data), which were present especially within the accumulation area of the CHN, where the lack of contrast in the ASTER imagery prevented accurate stereo matching. Selected parameters for DEM creation were: 50 m pixel size DEM; WGS-1984 datum; UTM-18S co-ordinates and mean sea level altitude reference. The ASTER-derived DEM covered most of the ablation zone of the CHN, but the main plateau was only partly represented. Areas with rough topography were also poorly covered due, we believe, to shadow effects and topography-induced image distortion on band 3B (Fig. 2). The resulting random error of the DEM was automatically calculated by PCI commercial software, by comparing the CPs and the resulting DEM, yielding 26 m. This error is composed of the errors in the CPs (19 m) and the uncertainties derived from the DEM generation process (19 m). Similar random error values have been obtained in DEMs generated for other mountain regions (Kääb, 2002). No bias was obtained in the distribution of errors, however, in the upper parts of the glaciers where the resulting ASTER-DEM is patchy and discontinuous, the error obtained in this paper (26 m) could be an underestimation. These areas were not covered in the previous cartography of the IGM, therefore, they are only marginally included in the analysis.

3.3. ELA

Casassa (1987) reported the equilibrium line altitude (ELA) of the CHN for Glaciares Nef and Soler as 1350 m asl. Aniya (1988), who used aerial photographs and field observations, defined the ELA for several glaciers, showing a significant west–east gradient, from 1200 m asl at Glaciares San Rafael and San Quintín to 1350 m asl at Glaciares Nef, Soler and Leones. In some cases, including Glaciares Benito and HPN-1, Aniya adopted the ELA of neighbouring glaciers.

Due to internannual meteorological variability and the temperate conditions in the CHN which results in strong melt (Matsuoka and Naruse, 1999), the ELA probably fluctuates widely from year to year. In the absence of direct measurements, the ELA for the glaciers of the CHN can be estimated based upon the assumption that the snow line at the end of the Southern Hemisphere summer (February–March) can be related to the ELA.

The ELA therefore was estimated based upon the observation of the snow line in the ASTER image mosaic of February 10, 2002 (Table 1). The ASTER image mosaic was digitally analysed based upon a false colour composite image (bands 1, 2 and 3N).

3.4. Areal, frontal and ice elevation changes

The total ice area in 1979 was manually digitised on screen from the Landsat MSS satellite image. This image covered most of the CHN with the exception of

Table 3
Glacier inventory (areas for year 2001), ELA (for year 2002) and area changes 1979–2001

Name	Margin of the CHN and type (*)	Total area (km^2)	Rock outcrops (km^2)	Ice area (km^2)	Debris-covered ice (km^2)	AAR	ELA m asl	Area change 1979–2001 (km^2)
Grosse	North (2)	78	12	66	28	0.54	1096	−1.4****
Exploradores	North (3)	95	9.6	86	15	0.64	1187	−3.2****
Bayo	North (3)	14	0.23	13	5.8	0.41	1206	n/d
U-6	East (3)	12	1.1	11	2.6	0.68	1267	−0.45
Fiero	East (2)	45	3	42	7.0	0.70	1294	−0.84
Mocho	East (2)	5.5	0.33	5.2	0.30	0.79	1148	−0.18
Cristal	East (3)	5.7	0.33	5.4		0.74	1329	−0.38
Leones	East (2)	73	7	66	3.2	0.74	1322	−0.85
Hyades	East (3)	7.9	0.23	7.6	0.09	0.83	1268	−0.16
Soler	East (3)	53	2.9	50	4.3	0.79	1283	−2.4
U-7	East (2)	2.0	0.25	1.3		0.90	1064	−0.24
Nef	East (2)	130	3.3	127	11	0.62	1183	−7.9
U-5	East (3)	5.3	0.33	5.0		0.62	1113	−1.2
Cachet Norte	East (3)	11	0.39	10		0.62	1145	−0.82
Cachet	East (2)	40	2.8	37		0.88	1303	−2.5
Colonia	East (2)	333	45.0	288	16	0.66	1302	−9.1
Arco	East (3)	28	1.9	26	0.53	0.84	1248	−0.44
Intermedio	East (3)	7.1	0.75	6.3		0.84	1350	−0.17
U-4	East (3)	15	1.9	13	0.68	0.63	1351	−0.64
Pared Norte	South (2)	84	3.9	80	7.8	0.53	1025	−1.0
Pared Sur	South (3)	35	3.4	32	6.9	0.48	975	−1.7
*****	South (2)	13	0.06	13		0.70	1065	−0.92
U-3	South (2)	18	0.47	18		0.78	1147	−0.47
U-2	South (3)	17	1.3	16	0.58	0.74	1136	−0.34
HPN-4	South (3)	71	5.5	65	0.45	0.60	1177	−2.0
Steffen	South (2)	454	26	428	3.7	0.57	1074	−12
Acodado	West (2)	274	5.2	269	0.22	0.64	1014	−12
HPN-1	West (3)	184	31	153	1.9	0.53	959	−9.5
Benito	West (2)	169	7.2	161	0.22	0.57	908	−7.2
Fraenkel	West (2)	33	1.8	31	0.37	0.69	1032	−1.8
Strindberg	West (3)	18	0.72	17		0.68	1008	−1.1
Andrée	West (3)	6.3	0.40	5.9		0.73	1032	−1.4
San Quintín	West (2)	795	5.2	790	0.38	0.71	957	−33
San Rafael	West (1)	741	19	722	0.33	0.85	1013	−14
Gualas	West (2)	141	22	119	8.5	0.57	1087	−3.2
*****	West (2)	84	13	72	7.4	0.59	1328	−4.2
Mormex	North (3)	3.1	0.54	2.6		0.78	1103	−0.18
Circo	North (3)	3.2	0.54	2.7		0.68	1262	−0.59
Verde	North (2)	7.6	0.58	7.0	0.79	0.63	1257	−0.89
**	(3)	53	3.4	50	0.19			
***	(3)	35		35				
Total		4197	244	3953	135	0.68 (average)	1150 (average)	−140

Notes: *1 tidewater, 2 freshwater, 3 non-calving.
**31 minor glaciers without names.
***Other glacier areas smaller than 0.5 km^2.
****Frontal area change 1975–2000 (Aniya, 2001).
*****These glaciers have been wrongly written "Piscis" and "Reicher" respectively, but the right names are due to the French geologist A. Pissis and the German explorer F. Reichert.
n/d, no available data.

the northern Glaciares Grosse and Exploradores. The ice extent in 2001 was measured based upon the Landsat ETM+ image, which was digitally analysed using the band ratio 4 to 5 (Paul et al., 2002). The debris-covered areas were manually digitised from the Landsat and ASTER image of February 2001.

The ice elevation changes were determined by subtracting the DEMs available for 1975 and 2001.

For that purpose, the pixels with extreme differences, regarded as erroneous data, were not included in the analysis. The rock areas were also excluded from the analysis.

3.5. Ice divides

The ice divides were manually mapped based on the DEM-2001 supplemented in flat areas without surface topography, with the analysis of ASTER and Landsat ETM+ images. This was accomplished with false colour composite image views as well as digitally-enhanced individual image band views, using the ice flow surface patterns, crevasses and moraines, in a similar way to the method of Aniya et al. (1996).

4. Results

4.1. Glacier inventory

The total area of the CHN was measured as 4197 km^2, based upon the Landsat ETM+ satellite image of 2001. This area is composed of 244 km^2 of rock outcrops, and 3953 km^2 total ice area, including adjacent small ice areas. The CHN was divided into 70 glaciers larger than 0.5 km^2 of ice-surface area. The adjacent, smaller ice areas were not treated individually, but accounted for a total marginal ice area of 35 km^2. The largest glaciers of the CHN are Glaciares San Quintín and San Rafael, at 790 and 722 km^2, respectively (Table 3). Together they represent 38% of the total ice area. The debris-covered areas were also distinguished, with a total area of 135 km^2 distributed mainly among Glaciares Grosse, Exploradores, Colonia and Nef (Table 3).

A total accumulation area ratio (AAR) of 0.68 was estimated for the CHN, with higher values among eastern glaciers, and smaller values for the northern glaciers (Table 3).

An average ELA position was estimated for each glacier (Table 3), yielding 1150 m asl as the overall ELA of the CHN. The spatial variation of the ELA fluctuated from minimum values in the western (1030 m asl) and southern glaciers (1090 m asl), to maximum altitude values obtained for the eastern glaciers (1250 m asl). The northern glaciers have an average ELA of 1190 m asl.

4.2. Area changes 1979–2001

A total ice-area loss of 140 km^2 between 1979 and 2001 was determined (3.4% of 1979 area). Assuming a worst case ice margin delineation error of +/− 1 pixel size (Williams et al., 1997) for both 1979 (57 m pixels) and 2001 (28.5 m pixels), multiplied by the ice area perimeter length of only the changed portion, we calculate worst case under/over-estimation errors of 54/61 km^2 respectively (+/− 1.5% of the 1979 area) for our estimate of ice-area change. This areal change corresponds mainly to the recession and shrinkage of western glaciers, which account for more than 62% of the total change. Among those glaciers experiencing the largest areal changes was Glaciar San Quintín, which lost 33 km^2 of ice area, particularly at its northern edge, where a new proglacial lake now occupies a former ice tongue (Fig. 1A).

Table 4
Average thinning rates measured at the ablation areas

Glacier name	Thinning rate (m a^{-1} ± 0.97)	% of ablation area with data
HPN-1	−4.0	46
Hyades	−3.3	56
Benito	−3.0	45
Soler	−2.5	54
Mocho	−2.5	82
Fraenkel	−2.4	90
Cachet	−2.2	91
Acodado	−2.1	72
U-6	−2.1	95
Gualas	−2.0	61
Fiero	−1.9	92
Nef	−1.9	63
San Quintín	−1.7	57
Cristal	−1.7	75
U-5	−1.7	83
Strindberg	−1.6	54
Steffen	−1.5	67
Cachet Norte	−1.5	98
Reichert	−1.4	34
Bayo	−1.3	56
Verde	−1.3	74
Leones	−1.2	89
Grosse	−1.1	94
Exploradores	−1.1	80
Colonia	−1.1	47

Area changes were found at most of the frontal tongues of the outlet glaciers of the CHN, but also at mid and higher elevations, where the ice was thinning and receding around most nunataks. This thinning and retreat process was particularly evident at the downstream (leeward) side of nunataks especially at Glaciares San Rafael and HPN-1.

The frontal tongues of calving glaciers were observed to be important sources of recession and area change. Some of the lower tongues collapsed into freshwater lakes, which expanded greatly beyond the 1979 ice-front position. Examples include the lakes associated with Glaciares Reichert, Cachet and Nef. Following the same trend, tidewater Glaciar San Rafael experienced an important frontal area change, with a linear retreat of

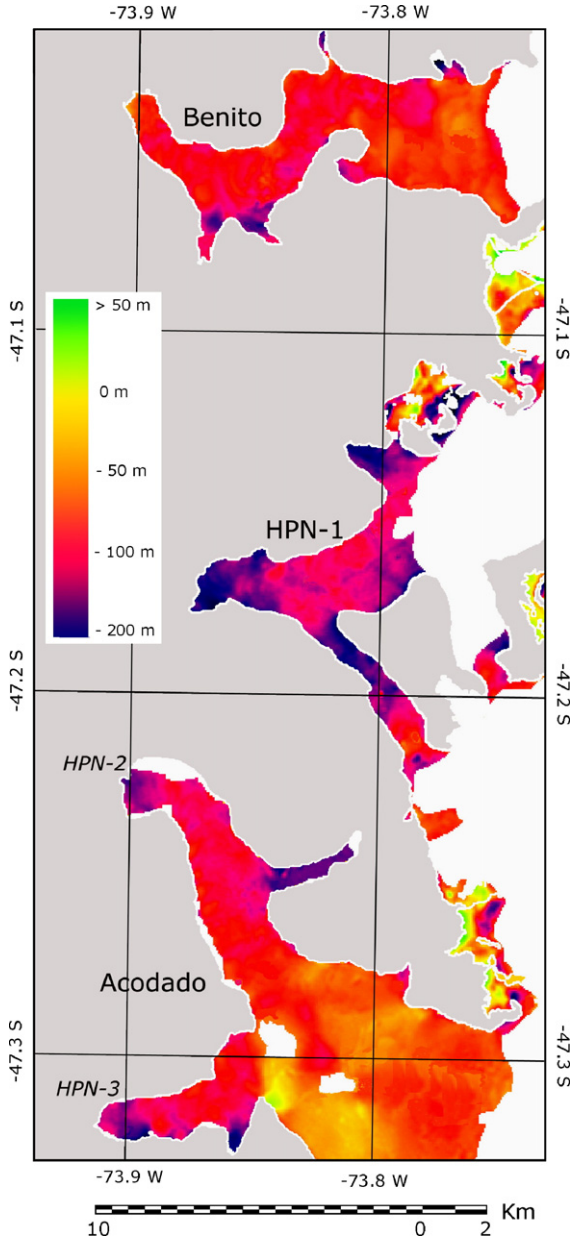

Fig. 3. Ice elevation change in m of western glaciers of the CHN, between 1975 and 2001. In grey, rock areas; in white, ice areas without data.

2250 m (84 m a^{-1}). This, together with the lateral area changes registered upstream, gave a total of 14 km^2 of ice-area loss since 1979 (the second largest of the CHN).

The non-calving glaciers have also been retreating and shrinking, for example, Glaciar Exploradores, whose lower end is debris covered. Exploradores' frontal tongue was stable between 1945 and 1991, when it began to retreat (Aniya, 2001) and several supraglacial lagoons appeared (Fernández, 2003). A similar process occurred on Glaciar Grosse, where most of the lower end of its debris-covered ablation area collapsed, in 1995/96, into a new proglacial lake that was generated by the agglomeration of small lagoons that appeared at the surface of the glacier due to melting and thinning of ice (Aniya and Wakao, 1997).

4.3. Ice elevation change

Due to the limited coverage of the 1975 cartography-derived DEM ('DEM-1975'), comparison with the 2001 ASTER-derived DEM ('DEM-2001') in order to identify ice elevation changes was restricted to the ablation areas and some of the lower parts of the accumulation zone, where the IGM cartography exhibited contour lines (Fig. 2). These upper areas were located mainly in the southern part of the CHN, and surrounding Monte San Valentín, where comparatively larger relief allowed photogrammetric restitution.

In order to ensure that detected changes in ice elevation were not spurious artefacts generated by the DEMs, we considered only those glacier areas for which the following criteria have been accomplished: (1) both DEMs provide the same topographic coverage over more than 25% of the area of interest (ice only, excluding rock); (2) ice elevation changes are higher than the combined DEM elevation error estimate (26 m); and (3) ice elevation changes are within a realistic range of few standard deviation, consistent with field experience (Rignot et al., 2003).

Examining the ablation areas using these criteria, it was possible to estimate an average thinning rate of -1.8 ± 0.97 m a^{-1} over ~50% of the total ablation areas of the CHN.

Ice thinning was observed in the ablation areas of glaciers located all around the CHN. A group of glaciers at the south-western margin exhibited a continuous

Table 5
Average thinning rates measured at the accumulation areas

Glacier name	Thinning rate (m $a^{-1}\pm0.97$)	% of accumulation area with data
Hyades	−3.5	66
U-7	−2.3	81
Mocho	−2.1	70
Soler	−2.0	25
U-6	−1.9	79
Bayo	−1.8	45
U-5	−1.6	72
Leones	−1.5	33
Fiero	−1.3	51
HPN-1	−1.2	39
Cachet Norte	−1.1	82
Nef	−1.1	39

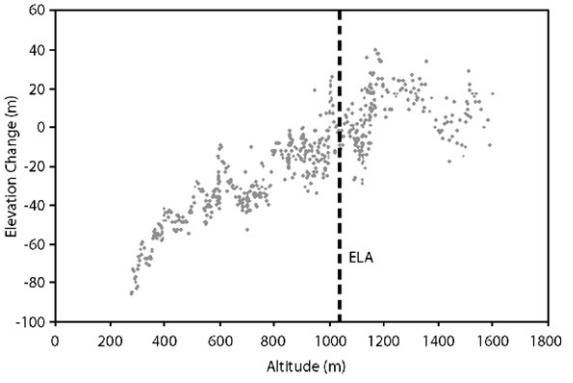

Fig. 4. Ice elevation changes of Glaciar Steffen, between 2001 and 1975 (y-axis, in m), and altitude of the glacier (x-axis in m asl). The vertical black line represents the ELA at a mean altitude of 1074 m asl based upon 2002 data.

spatial trend of thinning, with Glaciares HPN-1, Benito, Fraenkel and Acodado thinning at the highest rates (Table 4 and Fig. 3).

The accumulation areas were poorly covered in DEM-1975 and only patchily covered in the ASTER-DEM. A small proportion of CHN glacier accumulation areas did, however, satisfy our criteria for thinning analysis. These glaciers (Table 5), all showed thinning rates between -3.5 and -1.1 ± 0.97 m a^{-1}.

The relationship between ice elevation changes and altitude for all pixels of Glaciar Steffen (Fig. 4), showed a maximum thinning at low altitude and no change or even thickening in the accumulation areas. The observations of no change/thickening lie outside the criteria we have adopted to prevent possible false interpretation due to DEM error, and are therefore not definitive, although the observed pattern is similar to the curves obtained for several glaciers of the CHN and CHS by Rignot et al. (2003), and also is similar to curves obtained in other temperate glaciers in Alaska (Arendt et al., 2002).

5. Discussion

5.1. Icefield basins

In the previous glacier inventory of the CHN compiled by Aniya (1988), some ice basin boundaries were determined using the IGM 1975 maps, especially those located at the south-eastern end of the CHN (Pissis, Pared Norte and Sur among others). A large number of divides were, however, inferred from analysis of aerial photography, with very few identified from a limited field survey by Casassa (1987). Among the less clearly-defined ice divides were the boundaries between Glaciares San Quintín and Colonia, and between all south-western glaciers (Steffen, HPN-1, Benito, HPN-2 and HPN-3).

The ice divide between San Quintín and San Rafael obtained from our analysis of the ASTER-DEM and the Landsat ETM+ image was very similar to that described in the field by Casassa (1987). The divide between Glaciares San Quintín and Colonia (which is located in a flat plateau) was, however, located more than 6 km to the south compared to the divide defined by Aniya (1988). The area around this ice divide (Colonia–San Quintín) was partially covered by the ASTER-DEM, aiding a better definition of the boundary. The San Quintín ice basin defined here is very similar to that determined by Rignot et al. (2003), who used Space Shuttle Radar Topography Mission (SRTM) data.

Another area presenting difficulties for definition of ice divides was the south-western corner of the CHN, where several glaciers share a complex accumulation area. Some of these definitions, however, exhibit uncertainties which will only be resolved once it has been possible to perform more precise topographic or ice flow measurements. One area where it proved impossible to separate accumulation areas using the available data, was between Glaciares HPN-2 and HPN-3, which we prefer to treat as a single glacier under the name Glaciar Acodado, that being the name of the river draining the melt water generated by both glaciers (Fig. 1B).

5.2. Surface area

Aniya (1988) estimated the surface area of CHN from the 1974/75 aerial photographs and IGM maps as 4202 km^2, distributed over 28 main outlets, including rock outcrops. In his inventory, Aniya did not differentiate small glaciers (which were included within the main outlet glaciers), and he did not include 5 glaciers with an area of ice smaller than 5 km^2 each, which he considered were not part of the icefield.

The total 1974/75 CHN area, including rock outcrops, reported by Aniya (1988) is comparable with our own 2001 figure of 4197 km^2. This indicates broad agreement of areal estimates, although one would expect to see a larger value for the earlier measurement, given the observed thinning and retreat. Our ice area (excluding rock) estimate for 1979 is 4093 km^2 (Table 3: total ice area 2001 plus area change 1979–2001). Comparing this with Aniya's 1975 ice area total of 4020 km^2, our estimate for 1979 is 73 km^2 larger. This is contrary to expectations, given the observed retreat of most glaciers of the CHN during the 1970s (Aniya, 2001). We believe that the apparent disparity between our areal estimates and Aniya's can be explained by the omission of some

exposed rock areas by Aniya, as well as some possible underestimation of 1974/75 ice area.

As a result of the redefinition of ice divides in this study, some glacier basins like Colonia and HPN-1 appear more than 112 km^2 smaller than in Aniya's (1988) previous inventory, whilst Glaciar Acodado appears 106 km^2 larger than previously estimated. These discrepancies are probably related to the lack of topographic information and the unavailability of cloud-free satellite images, at the time when Aniya performed his inventory.

By comparing the remotely-sensed imagery from 1979 and 2001, it was possible to measure areal changes all around the glaciers, not only at the glacier fronts. Many lower-end tongues have previously been surveyed, although no prior consideration has been made of the ice-area changes experienced around nunataks within the accumulation areas, or those of the mid-altitude tongues. Aniya (2001) estimated that the ice-area change experienced by the CHN between 1975 and 2000 amounted to 54 km^2, or 2.2 $km^2\ a^{-1}$. This figure is only 34% of the total ice-area change measured in this work between 1979 and 2001 (140 km^2 or 6.4 $km^2\ a^{-1}$). We suggest that the large discrepancy is related to the fact that changes are occurring not only at the lower end of the glaciers as reported by Aniya, but are also occurring in the upper areas.

Between 1979 and 2001, not all glaciers experienced a linear trend of retreat. Some even advanced, for example Glaciar San Quintín, which advanced between 1991 and 1994 (Winchester and Harrison, 1996). Glaciar San Rafael retreated at high rates between 1974 and 1992 (Warren, 1993), after which the front become more stable. Between 1996 and 1999, several glaciers of the CHN were reported as advancing; for example Glaciares Gualas (Harrison and Winchester, 1998), Colonia (Harrison and Winchester, 2000) and San Rafael (Aniya 2001). In spite of these local advances, after 1999 most glaciers (including San Rafael and especially San Quintín) were retreating. In recent years, the lobate-type frontal tongue of Glaciar San Quintín has shown evidence of potential collapse into a proglacial lake, as predicted by Aniya and Wakao (1997).

5.3. Ice elevation and ELA change

The ice elevation changes measured in most of the ablation areas of the CHN in this study are similar to previous estimates and field measurements, although some large differences have been found in specific glaciers. For example, Aniya (1999) estimated the thinning of Glaciar HPN-1 as $-0.7\ m\ a^{-1}$ between 1945 and 1975, whilst we have found a thinning of $-4.0\ m\ a^{-1}$ between 1975 and 2001. The difference could be related to an acceleration of thinning in recent decades, as suggested by Rignot et al. (2003).

Our estimates of the ELA (based upon year 2002 data) for each glacier are similar to Aniya's (1988) results; however, some glaciers appear to have a much lower ELA at present, including most of the western glaciers. For example the ELA of Glaciares San Quintín, Benito and San Rafael is 240 m lower than Aniya's estimates. On the other hand, some glaciers seem to have a much higher ELA at present, especially those glaciers with avalanches zones or ice falls separating the accumulation and ablation areas, such as Reichert, Gualas, Fiero and Grosse. These differences are not necessarily a longer-term trend and are more probably indicators of inter-annual variability, or perhaps a result of inaccuracies in determining the ELA based on a single satellite image acquired at a certain epoch, which might not necessarily coincide with the time of maximum ablation.

5.4. Contribution to sea level rise

In order to account for the contribution of the CHN to sea level rise, Aniya (1999) estimated a total ice area lost of 64 km^2 between 1945 and 1996, and calculated an ice volume lost due to recession between 0.13 and 0.38 $km^3\ a^{-1}$. He then calculated the volume of ice lost due to thinning from the whole CHN, as 2.9 to 5.7 $km^3\ a^{-1}$. In total, his calculation of contribution to sea level rise yielded an average of 4.5 $km^3\ a^{-1}$ of ice between 1945 and 1996. This represents a sea level rise of 0.011 $mm\ a^{-1}$ of water equivalent.

Using the values obtained in this paper for the period 1979–2001, (140 km^2 of area lost; an average thinning rate of $-1.8\pm0.97\ m\ a^{-1}$ at the ablation zone of the CHN), our estimation of the contribution to sea level rise yielded an average of 5.7 $km^3\ a^{-1}$. This figure is within the upper estimation of Aniya (1999), but is ~25% higher than his average estimation. Furthermore, it is based on a trend that suggests acceleration of the thinning and shrinkage of ice. Multiplying by an average ice density of 850 $kg\ m^{-3}$ (Yamada, 1987), and dividing by the total surface of the ocean, this yields $0.013\pm0.006\ mm\ a^{-1}$ of water equivalent contributed between 1979 and 2001, the error being one standard deviation from the mean.

6. Conclusions

The high thinning rates obtained at the ablation (up to $-4.0\ m\ a^{-1}$) and accumulation areas (up to $-3.5\ m\ a^{-1}$), together with an area change between 1979 and 2001 of 140 km^2 of ice (3.4±1.5% of the 1979 total ice area), are

much larger than previous estimates for CHN. The more than double of areal change measured between 1979 and 2001 as compared with Aniya (1999) is basically explained by the inclusion in the analysis of nunataks and mid-altitude tongues of all the glaciers of the CHN. This higher areal change value suggests that changes are taking place all around the CHN, affecting the accumulation areas, as well as the ablation zones. The area changes at lower-altitude tongues are probably related as well to calving process, and therefore may become more dramatic in the short-term time scale. In the longer term, however, all glaciers are reacting similarly, exhibiting high thinning and retreat.

Taking into consideration all sources of ice wasting and using the higher thinning rates and larger areal changes presented here, the total contribution of the CHN to sea level rise was estimated to yield 0.013 ± 0.006 mm a^{-1}, ~25% higher than the previous estimation of Aniya (1999).

Whilst the quantitative accuracy of thinning rates derived from ASTER-DEM production is limited (±26 m), the DEM has nonetheless contributed to confirm the existence and trends of thinning, to make a reasonable estimate of the magnitude of thinning, and to assist in more detailed glaciological characterisation of the CHN. A more extensive analysis of glacier variations is required, in order to reduce uncertainties and measure in more detail the changes taking place within the CHN. This is particularly pertinent with respect to the accumulation areas, where few available data suggest that an important thinning process is taking place.

Acknowledgments

The contribution of satellite images by GLIMS, the USGS and GLCF is highly appreciated. This research is funded by project FONDECYT 1040515, CECS and Universidad de Chile. Intendencia Regional of Aysén provided access to the digital cartography of the CHN. CECS is funded by an Institute grant from the Millennium Science Initiative, the Tinker Foundation, Fundación Andes and by Empresas CMPC. Toby Benham is funded by the UK NERC Centre for Polar Observation and Modelling. The comments of the editor Christoph Schneider, one anonymous referee and Neil Glasser are acknowledged Fernando Ordenes helped with the figures.

References

Abrams, M., Hook, S., Ramachandran, B., 2002. ASTER User Handbook Version 2. Available online at: http://asterweb.jpl.nasa.gov/documents/aster_user_guide_v2.pdf.

Aniya, M., 1988. Glacier inventory for the Northern Patagonia Icefield, Chile, and variations 1944/45 to 1985/86. Arctic, Antarctic and Alpine Research 20 (2), 179–187.

Aniya, M., 1999. Recent glacier variations of the Hielos Patagónicos, South America, and their contribution to sea-level change. Arctic, Antarctic and Alpine Research 31 (2), 165–173.

Aniya, M., 2001. Glacier variations of Hielo Patagónico Norte, Chilean Patagonia, since 1944/45, with special reference to variations between 1995/96 and 1999/2000. Bulletin of Glaciological Research 18, 55–63.

Aniya, M., Wakao, Y., 1997. Glacier variations of Hielo Patagónico Norte, Chile, between 1944/45 and 1995/96. Bulletin of Glacier Research 15, 11–18.

Aniya, M., Sato, H., Naruse, R., Skvarca, P., Casassa, G., 1996. The use of satellite and airborne imagery to inventory outlet glaciers of the Southern Patagonia Icefield, South America. Photogrammetric Engineering and Remote Sensing 62, 1361–1369.

Arendt, A., Echelmeyer, K., Harrison, W., Lingle, C., Valentine, V., 2002. Rapid wastage of Alaska Glaciers and their contribution to rising sea level. Science 297, 382–386.

Casassa, G., 1987. Ice thickness deduced from gravity anomalies on Soler Glacier, Nef Glacier and the Northern Patagonia Icefield. Bulletin of Glacier Research 4, 43–57.

Falkner, E., 1995. Aerial Mapping. Methods and Applications. CRC Press Inc, USA. 322pp.

Fernández, A., 2003. Variaciones Recientes de Glaciares Ubicados entre 41° y 49° de Latitud Sur y su Relación con Cambios Climáticos. Unpublished thesis, Universidad de Chile, 210 pp.

Harrison, S., Winchester, V., 1998. Historical fluctuations of the Gualas and Reicher Glaciers, North Patagonian Icefield, Chile. The Holocene 8 (4), 481–485.

Harrison, S., Winchester, V., 2000. Nineteenth- and twentieth-century glacier fluctuations and climatic implications in the Arco and Colonia valleys, Hielo Patagónico Norte, Chile. Arctic, Antarctic and Alpine Research 32 (1), 55–63.

Heusser, C., 1960. Late-Pleistocene environments of the Laguna de San Rafael area, Chile. Geographical Review 50, 555–557.

Hutchinson, M., 1993. Development of a continent-wide DEM with applications for terrain and climate analysis. In: Goodchild, M., Parks, B., Steyaert, L. (Eds.), Environmental Modelling with GIS. Oxford University Press, pp. 392–399.

Kääb, A., 2002. Monitoring high-mountain terrain deformation from repeated air- and spaceborne optical data: examples using digital aerial imagery and ASTER data. ISPRS Journal of Photogrammetry and Remote Sensing 57 (1–2), 39–52.

Lythe, M., Vaughan, D., BEDMAP consortium, 2001. BEDMAP: a new ice thickness and subglacial topographic model of Antarctica. Journal of Geophysical Research 106 (b6), 11335–11351.

Matsuoka, K., Naruse, R., 1999. Mass balance features derived from a firn core at Hielo Patagónico Norte, South America. Arctic, Antarctic and Alpine Research 31 (4), 333–340.

Naruse, R., 1987. Characteristics of ice flow of Soler Glacier, Patagonia. Bulletin of Glacier Research 4, 79–85.

NIMA (National Imagery and Mapping Agency), 1997. Department of Defense World Geodetic System 1984: its definition and relationships with local geodetic systems. NIMA TR8350.2 Third Edition 4 July 1997. National Imagery and Mapping Agency, Bethesda, MD.

Paul, F., Kääb, A., Maisch, M., Kellenberger, T., Haeberli, W., 2002. The new remote sensing derived Swiss glacier inventory I: Methods. Annals of Glaciology 34, 355–362.

Rignot, E., Rivera, A., Casassa, G., 2003. Contribution of the Patagonia icefields of South America to global sea level rise. Science 302, 434–437.

Skvarca, P., De Angelis, H., Naruse, R., Warren, C., Aniya, M., 2002. Calving rates in fresh water: new data from southern Patagonia. Annals of Glaciology 34, 379–384.

Tucker, C., Grant, D., Dykstra, J., 2004. NASA's global orthorectified Landsat data. Photogrammetric Engineering and Remote Sensing 70 (3), 313–322.

Warren, C., 1993. Rapid recent fluctuations of the calving San Rafael Glacier, Chilean Patagonia: climatic or non-climatic? Geografiska Annaler 75A (3), 111–125.

Warren, C., Aniya, M., 1999. The calving glaciers of southern South America. Global and Planetary Change 22 (1–4), 59–77.

Warren, C., Sugden, D., 1993. The Patagonian icefields: a glaciological review. Arctic, Antarctic and Alpine Research 25 (4), 316–331.

Warren, C., Benn, D., Winchester, V., Harrison, S., 2001. Buoyancy-driven lacustrine calving, Glaciar Nef, Chilean Patagonia. Journal of Glaciology 47 (156), 135–146.

Williams, R., Hall, D., Sigurosson, O., Chien, Y., 1997. Comparison of satellite-derived with ground-based measurements of the fluctuations of the margins of Vatnajökull, Iceland, 1973–92. Annals of Glaciology 24, 72–80.

Winchester, V., Harrison, S., 1996. Recent oscillations of the San Quintín and San Rafael glaciers, Patagonian Chile. Geografiska Annaler 78a (1), 35–49.

Yamada, T., 1987. Glaciological characteristics revealed by 37.6-m deep core drilled at the accumulation area of San Rafael Glacier, the Northern Patagonia Icefield. Bulletin of Glacier Research 4, 59–67.

Yamaguchi, S., Naruse, R., Matsumoto, T., Ohno, H., 2003. Multiday variations in flow velocity at Glaciar Soler, Northern Patagonia, Chile. Arctic, Antarctic and Alpine Research 35 (2), 170–174.